

Band structure critical point energy in germanium–tin alloys with high tin contents

Cite as: Appl. Phys. Lett. **119**, 162102 (2021); doi: [10.1063/5.0064358](https://doi.org/10.1063/5.0064358)

Submitted: 22 July 2021 · Accepted: 5 October 2021 ·

Published Online: 19 October 2021



View Online



Export Citation



CrossMark

Dominic Imbrenda,¹ Rigo A. Carrasco,² Ryan Hickey,¹ Nalin S. Fernando,² Stefan Zollner,² and James Kolodzey^{1,a)}

AFFILIATIONS

¹Department of Electrical and Computer Engineering, University of Delaware, Newark, Delaware 19716, USA

²Department of Physics, New Mexico State University, Las Cruces, New Mexico 88003, USA

^{a)} Author to whom correspondence should be addressed: kolodzey@udel.edu

ABSTRACT

The dielectric functions of germanium–tin alloy thin-films, deposited by molecular beam epitaxy on bulk Ge substrates, with relatively high Sn contents from 15 to 27 at. %, were measured by variable angle spectroscopic ellipsometry over the wavelength range from 0.190 to 6 μm , using a combination of ultraviolet-visible and infrared ellipsometers. The band structure critical point energies, specifically the E_1 and $E_1 + \Delta_1$ optical transitions, were extracted from the measurements by a method of parametric oscillator modeling and second derivative analysis. With increasing Sn content, the transitions shifted to lower energies, and for alloys with less than 20% Sn, the numerical values agreed reasonably with predictions based on deformation potential theory that accounted for film strain. For the higher Sn alloys, the critical point energies from measurements agreed less well with deformation potential theory. These results provide information on the band structure of GeSn alloys with high Sn contents, which are increasingly important for long-wave infrared devices and applications.

Published under an exclusive license by AIP Publishing. <https://doi.org/10.1063/5.0064358>

Germanium–tin ($\text{Ge}_{1-x}\text{Sn}_x$) alloys are widely studied because of the many interesting properties they possess.^{1–5} For example, they are predicted to become direct bandgap semiconductors at a Sn percentage above around 6%–12%, depending on the strain state.^{3,6} As a Group IV direct bandgap material, they offer a potential route to a material compatible with Si and Ge fabrication processes for use in infrared optical devices, such as photodetectors,^{7–9} photoemitters,^{10–14} photoconductors,¹⁵ and lasers.^{16–18} At a Sn content above around 27%, the direct bandgap of relaxed $\text{Ge}_{1-x}\text{Sn}_x$ films is predicted to become zero,¹⁹ opening the possibility of exotic properties, compared to films with lower Sn content.²⁰

The optical constants of a semiconductor hold a rich amount of information about the electronic band structure. For example, the imaginary part of the dielectric function of germanium (Ge) exhibits several peaks and shoulders, which correspond to the energy levels of critical point transitions in the band structure: regions in k -space where there is a high probability of photon absorption.^{21–23} A comparison of the experimentally determined energy levels of the critical point transitions with calculations of the band structure can be used to test the accuracy of theoretical understanding.²² For example, several studies have been undertaken to determine the energy levels of the E_1 and $E_1 + \Delta_1$ critical point transitions in $\text{Ge}_{1-x}\text{Sn}_x$ alloys,^{19,24–26} but

most of these studies have focused on tin fractions with $x \leq 0.18$. More recently, the critical points of GeSn alloys with up to 33% Sn have been reported,^{27,28} but these alloys were deposited by chemical vapor deposition (CVD), whereas the alloys reported here, with up to 27% Sn, were deposited by molecular beam epitaxy (MBE) and may have somewhat different properties, including the amount of strain for a given film thickness, due to the lower growth temperature of MBE and the use of elemental rather than compound material sources.

To study the E_1 and $E_1 + \Delta_1$ optical transitions, four high Sn content $\text{Ge}_{1-x}\text{Sn}_x$ thin-film alloys with Sn atomic fractions $x = 0.15$ to 0.27 were deposited by MBE on Ge substrates and were characterized as described elsewhere.^{5,29} Structural parameters of the films used in this study, from Ref. 29, are given in Table I.

The samples in this study were optically characterized using variable angle spectroscopic ellipsometry (VASE) in the wavelength range from 0.190 to 6 μm , by a combination of ultraviolet-visible and infrared ellipsometers.²⁹ Since our samples comprised thin films grown on substrates, a four-layer structure was used for modeling the ellipsometric angles as a function of energy, including a vacuum ambient; a surface layer incorporating both surface roughness and any native oxide that may be present; the $\text{Ge}_{1-x}\text{Sn}_x$ film layer itself; and finally, a semi-infinite bulk Ge substrate. The dielectric function of the surface layer

TABLE I. Structural parameters of the GeSn films used in this study.²⁹ Sn% indicates the atomic percentage as determined from x-ray reciprocal space mapping (RSM). ϵ_{\parallel} and ϵ_{\perp} are the in-plane and out-of-plane film strain, respectively. Film relaxation is the ratio between the mismatch of the parallel lattice constants between the film surface and substrate, relative to that for a completely relaxed layer,³⁰ and is determined from RSM measurements. T_{sub} was the substrate temperature during MBE film deposition. Film thickness was determined from x-ray reflectivity (XRR). Surface roughness was determined from XRR and atomic force microscopy. The weighted mean squared error (MSE) gives the average deviation between the calculated and experimental ellipsometry data.

Sn (%)	ϵ_{\parallel} (%)	ϵ_{\perp} (%)	Relaxation (%)	T_{sub} (C°)	Film thickness (nm)	Surface roughness XRR (nm)	Surface roughness AFM (nm)	MSE
15	−1.02	0.78	54	120	42.5	1.00	0.62	0.92
18	−0.35	0.27	87	100	100.2	3.60	0.99	1.29
25	−0.12	0.17	96	100	132.9	1.46	1.83	1.46
27	−0.22	0.17	94	100	125.9	1.80	2.86	1.31

was obtained using an effective medium approximation layer that consisted of 50% film and 50% vacuum ambient. A Kramers–Kronig (K–K) consistent Johs-Herzinger parametric oscillator model, consisting of eight oscillators with multiple fitting parameters (about 40 total), was employed to model the $\text{Ge}_{1-x}\text{Sn}_x$ film layer and the Ge substrate, as explained previously.²⁹ Several iteration cycles of modeling were performed for converging to accurate parameters, including the layer thicknesses. A model fit was considered satisfactory when the MSE was minimized, which is the mean square difference between the measured and modeled ellipsometric angles, normalized to the standard deviation of experimental error, and given in Table I.

This VASE experiment measures the ordinary dielectric function (electric field vector within the layer growth plane) and is not sensitive to the extraordinary dielectric function (electric field vector along the layer surface normal, which is also the optical axis).³¹ Since the residual strain is small (from Table I), the differences between the ordinary and extraordinary dielectric functions (and the resulting impact on critical point energies) will also be small.³² As explained previously, the strain splittings and energy shifts are much smaller than the spin-orbit splitting.¹⁹ Plots of the dielectric functions of all these samples were published previously.²⁹

The parametric oscillator model has been successfully used to determine the optical properties of many semiconductors,³³ but because of strong correlations between parameters, two solutions with different fitting parameters (e.g., energies) could, in principle, yield similar dielectric function dispersions. To ensure that any observed features were intrinsic to the materials and not artifacts of the modeling, a second fitting method for the dielectric functions was employed, and the results compared to the first fitting described above. In this second method, the layer thicknesses were fixed at the values from the first fit, and the real and imaginary parts of the film's dielectric function were adjusted again to the data at each measured energy. A fitting performed in this manner is known as a point-by-point fit and is not necessarily K-K consistent. When the optical constants obtained from the point-by-point fits were compared to those obtained from the first parametric oscillator fitting, the results were nearly identical, providing confidence with the validity of both fitting methods. Because the point-by-point fit is not constrained by smooth curves, it may describe more accurately the subtler features of the dielectric function and, therefore, was used for the second derivative analysis, as described below.^{21,24,33,34}

Starting with the dielectric constants obtained from the point-by-point fitting, the second derivatives were obtained by numerical

differentiation and then smoothed to reduce noise in the calculated line shape using 10 Savitzky–Golay coefficients, which fit a smoothed curve to noisy data using a least squares procedure.³⁵ The number of Savitzky–Golay coefficients were determined by the signal-to-noise ratio of the measured data, where higher noise required more coefficients; there was a trade-off between using enough coefficients to obtain a smooth curve, but not to distort the calculated line shape. The E_1 critical point is in the region of k -space near the L point in the Λ (the [111]) crystallographic direction, where the conduction and valence bands are nearly parallel; the $E_1+\Delta_1$ is the transition from the split-off valence band to the conduction band in the same k -space region. In Ge, the E_1 and $E_1+\Delta_1$ critical points of the joint density of states can be described as a mixture of a 2D minimum and a saddle point Van Hove singularity.^{24,34} A logarithmic line shape analytical expression can describe such a singularity and was used to fit the energy level of each critical point transition to the dielectric spectra,³⁶ with the second derivative of the line shape for a mixture of a 2D minimum and saddle point given by,^{23,37}

$$\frac{d^2\epsilon}{dE^2} = \sum_j \frac{A_j e^{i\Phi_j}}{(E - E_j + i\Gamma_j)^2}, \quad (1)$$

where the fitting parameters are as follows: E_j is the critical point energy of the transition, A_j is the amplitude for transition j , Γ_j is the broadening for transition j , and Φ_j is the excitonic phase angle, which describes the contribution of excitonic effects to the critical point and the level of mixing.³⁴ To determine the fitting parameters in Eq. (1) for each film, the summation was taken over both the E_1 and $E_1+\Delta_1$ transitions, and the real and imaginary parts of the derivative of each dielectric function were solved simultaneously using a least squares procedure based on the Levenberg–Marquardt method.³⁸ Initially, the excitonic phase angle Φ_j was forced to take the same value in both the E_1 and $E_1+\Delta_1$ transitions^{19,36} but relaxed during subsequent iterations. Typical fits of Eq. (1) to the numerically calculated derivatives of the dielectric function modeled by the point-by-point fit are given in Fig. 1 for the 15% and the 25% Sn content films. The amplitude, broadening, excitonic phase angle, and energy fitting parameters for each film are given in Table II. While fitting the derivative data to the E_1 and $E_1+\Delta_1$ critical points for the 15% and 25% Sn films, the spectral range was restricted to 1.7–2.2 eV and 1.5–2.2 eV, respectively, to ensure that contributions from other critical point transitions did not overlap. The fittings for the other composition films (not shown) were performed in an identical manner, with the spectral ranges also restricted to just

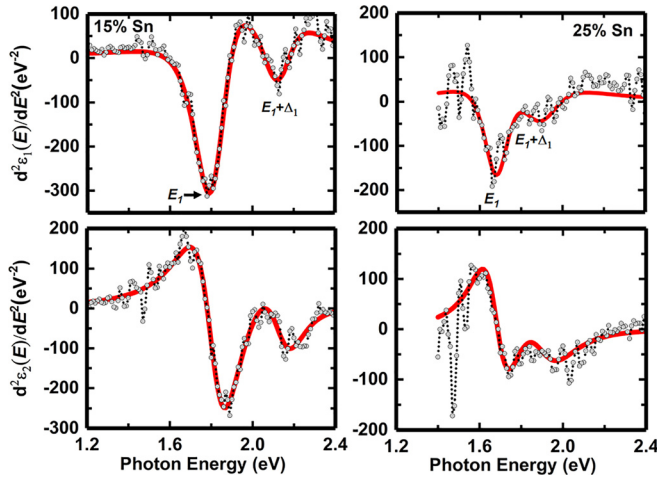


FIG. 1. Second derivative of the real and imaginary parts of the dielectric function (ϵ_1 and ϵ_2 , respectively) vs photon energy of the (a) 15% Sn content film (left column) and (b) 25% Sn content film (right column). Symbols and dotted lines are the values numerically calculated from the point-by-point fit data, and the solid lines are the fitting using the analytical expression of Eq. (1) over limited energy ranges. The dotted line is a visual aid only. The approximate locations of the E_1 and $E_1+\Delta_1$ critical point transitions are indicated for ϵ_1 for each film.

account for their E_1 and $E_1+\Delta_1$ critical points. Based on the accuracy of the measured ellipsometric angles, and an analysis of the fitting procedures for extracting the dielectric parameters, we estimate that the error of the critical point energies is below 0.001 eV for the samples with less than 20% Sn, and below 0.01 eV for the samples with more than 20% Sn.

The fluctuations and oscillations surrounding the analytical fitting curves in Fig. 1 were higher for the 25% Sn sample than for the 15% Sn sample. The likely reasons include (a) non-uniform layer

TABLE II. Extracted parameters used to fit Eq. (1) to the derivatives of the dielectric function obtained from the point-by-point modeling of the VASE experimental data for the GeSn samples used in the study.

E_1 transition				
Sn (%)	Energy (eV)	Amplitude, A	Broadening, Γ (eV)	Phase angle, Φ (deg)
15	1.816	46.65	0.14	211
18	1.742	40.02	0.18	210
25	1.685	19.51	0.12	188
27	1.711	13.50	0.24	188
$E_1+\Delta_1$ transition				
Sn (%)	Energy (eV)	Amplitude, A	Broadening, Γ (eV)	Phase angle, Φ (deg)
15	2.137	14.74	0.13	210
18	2.030	14.56	0.14	210
25	1.893	11.94	0.17	188
27	1.933	5.051	0.14	188

thickness, for example, due to variations in the growth temperature or molecular flux across the sample; (b) surface roughness; (c) defects near the substrate/layer interface; and (d) other defects in the layer, such variations in the Sn content throughout the layer. These effects begin to break down the assumptions of layer homogeneity and plan-parallel interfaces, which are required for Fresnel's equations to be valid. Therefore, some oscillations will occur in the extracted (point-by-point) dielectric function of the sample, and artifacts will appear in the dielectric function that will be amplified in the second derivative. Nevertheless, the numerical derivatives of the dielectric function for the 25% sample still show pronounced van Hove singularities, which can clearly identify the parameters of the critical points. The ellipsometry data for the 27% Sn percentage film unfortunately had a low signal-to-noise ratio at lower photon energies (<1.8 eV) and required a higher level of smoothing when the second derivative was calculated, relative to the lower Sn samples.

It is interesting to compare the critical point energies for the current high Sn content films with extrapolations from the prior studies of lower Sn content films. Films with different thickness and composition, however, will have different degrees of strain, which must be accounted for to predict the correct energies. Therefore, the comparisons here will be based on extrapolations from *relaxed* films, which are then subsequently adjusted for the strain in the measured films. For *relaxed* $\text{Ge}_{1-x}\text{Sn}_x$ alloys, the compositional dependence of the E_1 and $E_1+\Delta_1$ energy transitions can be empirically expressed as¹⁹

$$E_1(x) = E_1^{\text{Ge}}(1-x) + E_1^{\alpha\text{Sn}}x - b_{E_{\text{GeSn}}}x(1-x), \quad (2)$$

where E_1^{Ge} and $E_1^{\alpha\text{Sn}}$ are the E_1 energy values for bulk Ge and αSn , respectively, and $b_{E_{\text{GeSn}}}$ is a bowing parameter that accounts for the non-linearity of the interpolation. The $E_1+\Delta_1$ transition is determined in a similar manner by replacing the subscript "1" with "1+ Δ_1 ." Values for critical point transition energies and bowing parameters were taken from Ref. 19 and are given in Table III. To adjust for the compressive strain, which increased the energy levels of the E_1 and $E_1+\Delta_1$ transitions from their relaxed values, the perturbation was determined here by deformation potential theory (DPT).³⁹ The strain dependence of the critical points is given by¹⁹

$$E_1^s = E_1^r + \frac{\Delta_1}{2} + \Delta E_H - \sqrt{\frac{(\Delta_1)^2}{4} + (\Delta E_S)^2}, \quad (3)$$

$$(E_1 + \Delta_1)^s = (E_1 + \Delta_1)^r - \frac{\Delta_1}{2} + \Delta E_H + \sqrt{\frac{(\Delta_1)^2}{4} + (\Delta E_S)^2}, \quad (4)$$

where the superscripts s and r indicate values for the strained and relaxed alloys, respectively, and Δ_1 is the spin-orbit splitting of the valence band at the L point for Ge, taken as the difference between the

TABLE III. Critical point energies, bowing parameters, and spin-orbit splitting energy for Ge and Sn. All values are in units of eV.¹⁹

	Ge	Sn	$b_{E_{\text{GeSn}}}$
E_1	2.120	1.270	1.650
$E_1+\Delta_1$	2.310	1.770	1.050
Δ_1	0.190	0.50	-0.60

E_1 and $E_1 + \Delta_1$ critical point energy levels for Ge, given in Table III. ΔE_H and ΔE_S are energy shifts due to the hydrostatic and shear strain, obtained using the methods described in Ref. 19, and the strain data used to determine these parameters for each film are given in Table I. For Eqs. (3) and (4), the shift from hydrostatic strain, ΔE_H , and shear strain, ΔE_S , were calculated by¹⁹

$$\Delta E_H = \sqrt{3}D_1^1\epsilon_H, \quad (5)$$

$$\Delta E_S = \sqrt{6}D_3^3\epsilon_S, \quad (6)$$

where $D_1^1 = -5.4$ eV and $D_3^3 = -3.8$ eV¹⁹ are the hydrostatic and shear deformation potentials, respectively, for $\text{Ge}_{1-x}\text{Sn}_x$ alloys with $x \leq 0.17$,²⁵ and ϵ_H and ϵ_S are the hydrostatic and shear strains of the film calculated from Table I. For $\text{Ge}_{1-x}\text{Sn}_x$ alloys with higher Sn fraction, the deformation potentials may deviate slightly from the values given above for lower $x \leq 0.17$.

The energy levels of the E_1 and $E_1 + \Delta_1$ critical points determined from the second derivative fittings vs Sn fraction, as well as comparisons with other published data, are given in Fig. 2. The circles in Fig. 2 are the experimental critical point energies determined from ellipsometry measurements on the samples reported here. The dashed lines are the energy values for each critical point transition as a function of alloy Sn fraction for relaxed $\text{Ge}_{1-x}\text{Sn}_x$ alloys, calculated by the empirical Eq. (2). If the alloy films in this study were completely relaxed, the critical point transition energies should lie on these dashed lines, whereas the films in this study were strained. The squares in Fig. 2 are the predicted energy values for each of the strained films in this study, calculated from the relaxed film values by DPT using Eqs. (3) and (4), and the strain data in Table I. The DPT strain corrections were relatively small, and the energies matched the experimental critical point energies determined from ellipsometry reasonably well for the 15% and 18% Sn films. The authors of a previous study⁴⁰ performed an

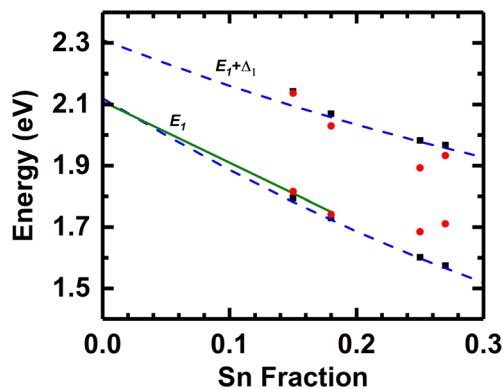


FIG. 2. Critical point energies for E_1 and $E_1 + \Delta_1$ vs Sn content of the MBE-grown $\text{Ge}_{1-x}\text{Sn}_x$ alloys. Circles are the energy values determined from fitting experimentally measured ellipsometry data to Eq. (1); dashed lines are the energy values predicted from Eq. (2) for relaxed alloys,¹⁸ square symbols are energy values predicted by deformation potential theory for strained alloys using the experimentally measured value of strain, and the solid line is the predicted E_1 energy using the compositionally dependent empirical fit from Ref. 40 as explained in the text. Values determined from ellipsometry (circles) compare reasonably well with predicted values (squares) for all samples except for the 25% and the 27% Sn samples.

empirical fitting of the E_1 energy transition for pseudomorphically strained films on Ge substrates with Sn contents from 0% to 17%, and this fit is included in Fig. 2 by the solid line, for comparison. Note that for the E_1 transition, the third and fourth terms in Eq. (3) tended to cancel each other,²⁵ and the effect of strain on the energy transition level was minimized. For example, the 15% Sn content film is only 54% relaxed, whereas the 18% Sn content film is 87% relaxed, yet the E_1 energy values for both films predicted from Eqs. (3) and (4) differ by only about 1% from the relaxed film values of Eq. (2).

For the 25% and the 27% Sn films, there were greater differences (up to about 0.1 eV) between the experimental ellipsometry values (circles) and the values theoretically predicted from DPT (squares). We speculate that possible causes of the deviations for the 25% and 27% Sn films may include uncertainties in the deformation potentials as discussed for Eqs. (5) and (6) above; numerical instabilities and distortions of the calculated second derivative line shape due to the smoothing filter that was applied; incomplete removal of optical interference effects from the substrate; experimental measurement errors; and uncertainties in the transition energies in high-Sn samples.⁴¹ Another possibility is the occurrence of short-range order (SRO) that modifies the atomic bonding probabilities from that of a random alloy, and which has been reported to affect the band energies, particularly for a Sn content above about 10%.⁴² No trends were evident in the dependence of split-off band separation Δ_1 vs the Sn content.

If applied correctly, both MBE and chemical vapor deposition can produce high-quality homogeneous layers of Ge-Sn alloys with high Sn content. The dielectric functions and derivatives of high-Sn alloys grown by CVD show results similar to those of the MBE-grown GeSn alloys described here, with no significant differences in the optical properties of layers, which is interesting considering that the MBE films were grown at substrate temperatures of 100 to 120 °C, whereas the CVD films were grown at 240 to 290 °C, and also that MBE uses elemental sources but CVD uses specialty precursor compounds.^{27,28}

In summary, the E_1 and $E_1 + \Delta_1$ critical point energies for $\text{Ge}_{1-x}\text{Sn}_x$ alloys with Sn atomic fractions $x = 0.15$ to 0.27 were evaluated from VASE measurements. These energies were determined by fitting the second derivative of the complex dielectric spectra to an analytical model of a 2D minimum and a saddle point Van Hove singularity. The energy levels from the VASE fitting were also compared to predictions from DPT¹⁹ and empirical results. The energies matched well with the predicted levels except for the higher Sn content films.

The parameters evaluated in this study can be compared to future *ab initio* calculations of the band structure of GeSn alloys to determine the validity of the theoretical calculations and also used as a guide to predict critical point transitions in even higher Sn concentration alloys, which are becoming important for long-wave infrared applications.

This work was funded in part by grants from the Air Force (AFOSR Award Nos. FA9550-14-1-0207, FA9550-13-1-0022, and FA9550-17-1-0134), the Army Research Office (ARO Award No. W911NF-12-1-0380), and by gifts from Thorlabs, Inc. Special thanks to T. N. Adam, D. T. Beatson, B. B. Claflin, C. Duong, A. M. Kiefer, R. Soref, T. Wang, and S.-Q. (Fisher) Yu, for valuable discussions.

DATA AVAILABILITY

The data that support the findings of this study are available from the corresponding author upon reasonable request.

REFERENCES

- ¹S. Wirths, D. Buca, and S. Mantl, *Prog. Cryst. Growth Charact. Mater.* **62**, 1 (2016).
- ²J. Kouvetakis, J. Menendez, and A. V. G. Chizmeshya, *Annu. Rev. Mater. Res.* **36**, 497 (2006).
- ³S. Gupta, B. Magyari-Köpe, Y. Nishi, and K. C. Saraswat, *J. Appl. Phys.* **113**, 073707 (2013).
- ⁴P. Moontragoon, R. A. Soref, and Z. Ikonik, *J. Appl. Phys.* **112**, 073106 (2012).
- ⁵R. Hickey, N. Fernando, S. Zollner, J. Hart, R. Hazbun, and J. Kolodzey, *J. Vac. Sci. Technol. B* **35**, 021205 (2017).
- ⁶H. Lin, R. Chen, W. Lu, Y. Huo, T. I. Kamins, and J. S. Harris, *Appl. Phys. Lett.* **100**, 141908 (2012).
- ⁷S. Kim, N. Bhargava, J. Gupta, M. Coppinger, and J. Kolodzey, *Opt. Express* **22**, 11029 (2014).
- ⁸Y. Dong, W. Wang, D. Lei, X. Gong, Q. Zhou, S. Y. Lee, W. K. Loke, S.-F. Yoon, E. S. Tok, G. Liang, and Y.-C. Yeo, *Opt. Express* **23**, 18611 (2015).
- ⁹W. Wang, S. Vajandar, S. L. Lim, Y. Dong, V. R. D'Costa, T. Osipowicz, E. S. Tok, and Y. C. Yeo, *J. Appl. Phys.* **119**, 155704 (2016).
- ¹⁰J. P. Gupta, N. Bhargava, S. Kim, T. Adam, and J. Kolodzey, *Appl. Phys. Lett.* **102**, 251117 (2013).
- ¹¹W. Du, Y. Zhou, S. A. Ghetmiri, A. Mosleh, B. R. Conley, A. Nazzal, R. A. Soref, G. Sun, J. Tolle, J. Margetis, H. A. Naseem, and S.-Q. Yu, *Appl. Phys. Lett.* **104**, 241110 (2014).
- ¹²R. Roucka, J. Mathews, R. T. Beeler, J. Tolle, J. Kouvetakis, and J. Menendez, *Appl. Phys. Lett.* **98**, 061109 (2011).
- ¹³H. H. Tseng, K. Y. Wu, H. Li, V. Mashanov, H. H. Cheng, G. Sun, and R. A. Soref, *Appl. Phys. Lett.* **102**, 182106 (2013).
- ¹⁴M. Oehme, K. Kostecky, T. Arguirov, G. Mussler, K. Ye, M. Gollhofer, M. Schmid, M. Kaschel, R. A. Korner, M. Kittler, D. Buca, E. Kasper, and J. Schulze, *IEEE Photonics Technol. Lett.* **26**, 187 (2014).
- ¹⁵J. Hart, T. Adam, Y. Kim, Y. C. Huang, A. Reznicek, R. Hazbun, J. Gupta, and J. Kolodzey, *J. Appl. Phys.* **119**, 093105 (2016).
- ¹⁶S. Wirths, R. Geiger, N. Von Den Driesch, G. Mussler, T. Stoica, S. Mantl, Z. Ikonik, M. Luysberg, S. Chiussi, J. M. Hartmann, H. Sigg, J. Faist, D. Buca, and D. Grützmacher, *Nat. Photonics* **9**, 88 (2015).
- ¹⁷S. Al-Kabi, S. A. Ghetmiri, J. Margetis, T. Pham, Y. Zhou, W. Dou, B. Collier, R. Quinde, W. Du, A. Mosleh, J. Liu, G. Sun, R. A. Soref, J. Tolle, B. Li, M. Mortazavi, H. A. Naseem, and S. Q. Yu, *Appl. Phys. Lett.* **109**, 171105 (2016).
- ¹⁸Y. Zhou, Y. Miao, S. Ojo, H. Tran, G. Abernathy, J. M. Grant, S. Amoah, G. Salamo, W. Du, J. Liu, J. Margetis, J. Tolle, Y. Zhang, G. Sun, R. A. Soref, B. Li, and S.-Q. Yu, *Optica* **7**, 924 (2020).
- ¹⁹N. S. Fernando, R. A. Carrasco, R. Hickey, J. Hart, R. Hazbun, S. Schoeche, J. N. Hilfiker, J. Kolodzey, and S. Zollner, *J. Vac. Sci. Technol. B* **36**, 021202 (2018).
- ²⁰H. S. Lan, S. T. Chang, and C. W. Liu, *Phys. Rev. B* **95**, 201201 (2017).
- ²¹G. Jungk, *Phys. Status Solidi* **67**, 85 (1975).
- ²²M. Cardona and P. Y. Yu, *Fundamentals of Semiconductors* (Springer-Verlag, Berlin Heidelberg, 2005).
- ²³M. Cardona, *Modulation Spectroscopy* (Academic Press, New York, 1969).
- ²⁴V. R. D'Costa, C. S. Cook, A. G. Birdwell, C. L. Littler, M. Canonico, S. Zollner, J. Kouvetakis, and J. Menéndez, *Phys. Rev. B* **73**, 125207 (2006).
- ²⁵V. R. D'Costa, W. Wang, Q. Zhou, E. Soon Tok, and Y. C. Yeo, *Appl. Phys. Lett.* **104**, 022111 (2014).
- ²⁶M. Medikonda, G. R. Muthinti, R. Vasić, T. N. Adam, A. Reznicek, M. Wormington, G. Malladi, Y. Kim, Y.-C. Huang, and A. C. Diebold, *J. Vac. Sci. Technol. B* **32**, 061805 (2014).
- ²⁷C. Xu, D. Ringwala, D. Wang, L. Liu, C. D. Poweleit, S. L. Y. Chang, H. L. Zhuang, J. Menéndez, and J. Kouvetakis, *Chem. Mater.* **31**, 9831 (2019).
- ²⁸C. Xu, P. M. Wallace, D. A. Ringwala, S. L. Y. Chang, C. D. Poweleit, J. Kouvetakis, and J. Menéndez, *Appl. Phys. Lett.* **114**, 212104 (2019).
- ²⁹D. Imbrenda, R. Hickey, R. A. Carrasco, N. S. Fernando, J. VanDelslice, S. Zollner, and J. Kolodzey, *Appl. Phys. Lett.* **113**, 122104 (2018).
- ³⁰W. X. Ni, K. Lyutovich, J. Alami, C. Tengstedt, M. Bauer, and E. Kasper, *J. Cryst. Growth* **227–228**, 756 (2001).
- ³¹D. E. Aspnes, *J. Opt. Soc. Am.* **70**, 1275 (1980).
- ³²S. Zollner, in *SiGeC Alloys and Their Applications*, edited by S. Pantelides and S. Zollner (Gordon & Breach Science Publishers, SA, 2002).
- ³³C. Xu, C. L. Senaratne, J. Kouvetakis, and J. Menéndez, *Solid State Electron.* **110**, 76 (2015).
- ³⁴L. Viña, S. Logothetidis, and M. Cardona, *Phys. Rev. B* **30**, 1979 (1984).
- ³⁵A. Savitzky and M. J. E. Golay, *Anal. Chem.* **36**, 1627 (1964).
- ³⁶S. M. Kelso, D. E. Aspnes, M. A. Pollack, and R. E. Nahory, *Phys. Rev. B* **26**, 6669 (1982).
- ³⁷D. E. Aspnes, *Surf. Sci.* **37**, 418 (1973).
- ³⁸T. N. Nunley, N. S. Fernando, N. Samarasingha, J. M. Moya, C. M. Nelson, A. A. Medina, and S. Zollner, *J. Vac. Sci. Technol. B* **34**, 061205 (2016).
- ³⁹J. Bardeen and W. Shockley, *Phys. Rev.* **80**, 72 (1950).
- ⁴⁰V. R. D'Costa, W. Wang, Q. Zhou, T. K. Chan, T. Osipowicz, E. S. Tok, and Y. C. Yeo, *J. Appl. Phys.* **116**, 053520 (2014).
- ⁴¹R. A. Carrasco, S. Zollner, S. A. Chastang, J. Duan, G. J. Grzybowski, B. B. Claffin, and A. M. Kiefer, *Appl. Phys. Lett.* **114**, 062102 (2019).
- ⁴²B. Cao, S. Chen, X. Jin, J. Liu, and T. Li, *ACS Appl. Mater. Interfaces* **12**, 57245 (2020).